Electronic Supplementary Material (ESI) for Chemical Science.

Citrate-based fluorescent materials for low-cost chloride sensing in the diagnosis of Cystic Fibrosis

Jimin P. Kim[1], Zhiwei Xie[1], Michael Creer[2], Zhiwen Liu[3], Jian Yang[1,*]

[1] Department of Biomedical Engineering, Materials Research Institutes, the Huck Institutes of Life Sciences, The Pennsylvania State University, University Park, PA 16802

[2] Department of Pathology, College of Medicine, The Pennsylvania State University, Hershey, PA 17033

[3] Department of Electrical Engineering, The Pennsylvania State University, University Park, PA 16802

* To whom correspondence should be addressed. Email: jxy30@psu.edu

Table of Contents

Section A: Supplementary Figures

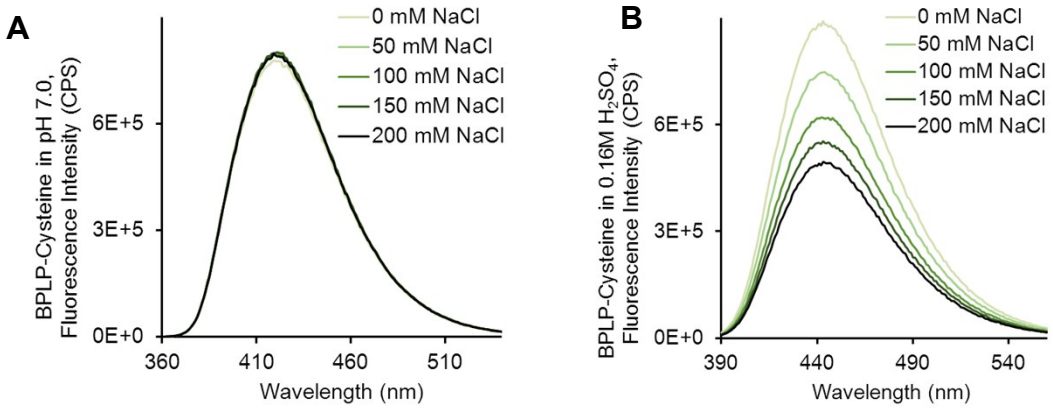

Figure S1. Chloride sensitivity of BPLP-Cysteine pre-polymer in solution. (A) BPLP-Cysteine (0.1 O.D.) in pH 7.0 phosphate buffer showed no quenching (at 1 nm bandpass), while (B) significant quenching of fluorescence was observed in pH 0.77 (0.16M H_2SO_4) (0.1 O.D., 1.1 nm bandpass).

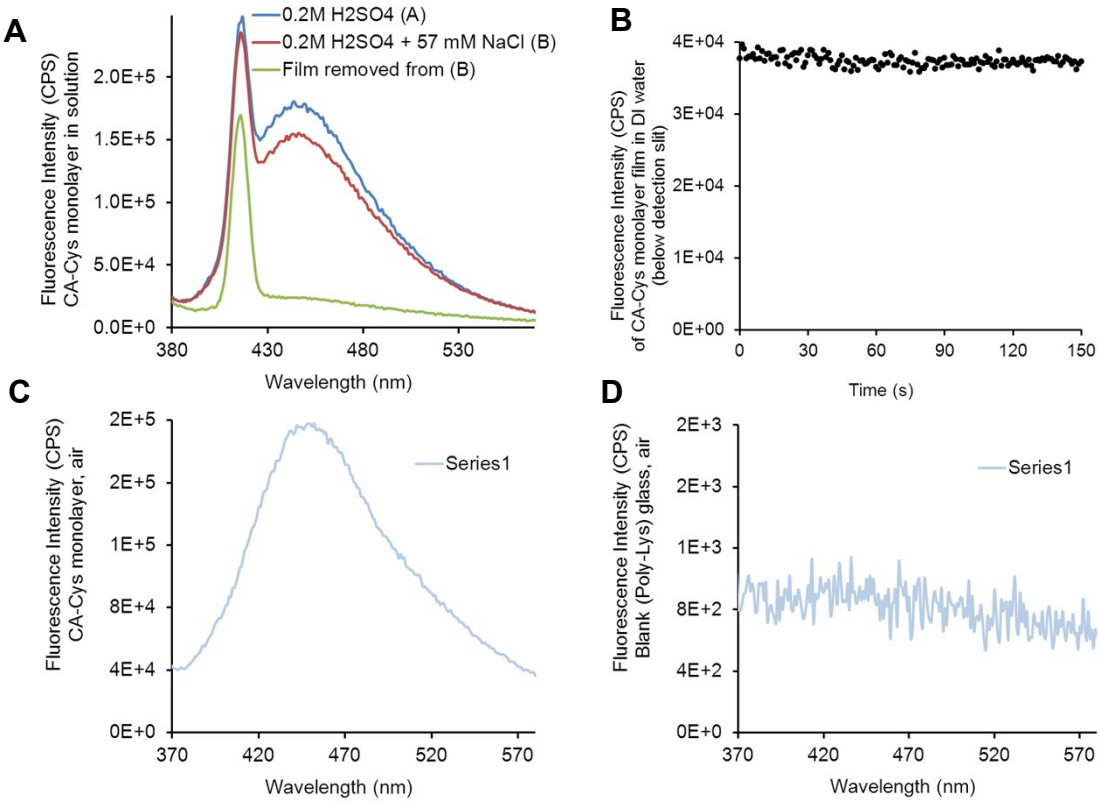

Figure S2. Chloride sensitivity of immobilized monolayer of CA-Cysteine. (A) Monolayer film of CA-Cysteine was immobilized onto poly-Lys coated glass by EDC/NHS coupling, demonstrating fluorescence quenching by chloride under acidic conditions (with dye concentration kept constant). To obtain chloride sensitivity, we removed the coated film to account for background fluorescence from CA-Cysteine released into solution, which was minimal. Chloride sensitivity (Ksv) was 3.145, similar to that obtained in Fig. S1, and similar

results were obtained with a thin layer of crosslinked BPLP-Cysteine (3 days at 80ºC). (B) Kinetic measurement of the release rate of CA-Cysteine from the immobilized coating, showing minimal release (that may contribute to chloride sensitivity in (A). (C) Demonstrating solid state fluorescence of the immobilized monolayer of CA-Cysteine. (D). Fluorescence of poly-Lys coated glass control (with no conjugation of CA-Cysteine).

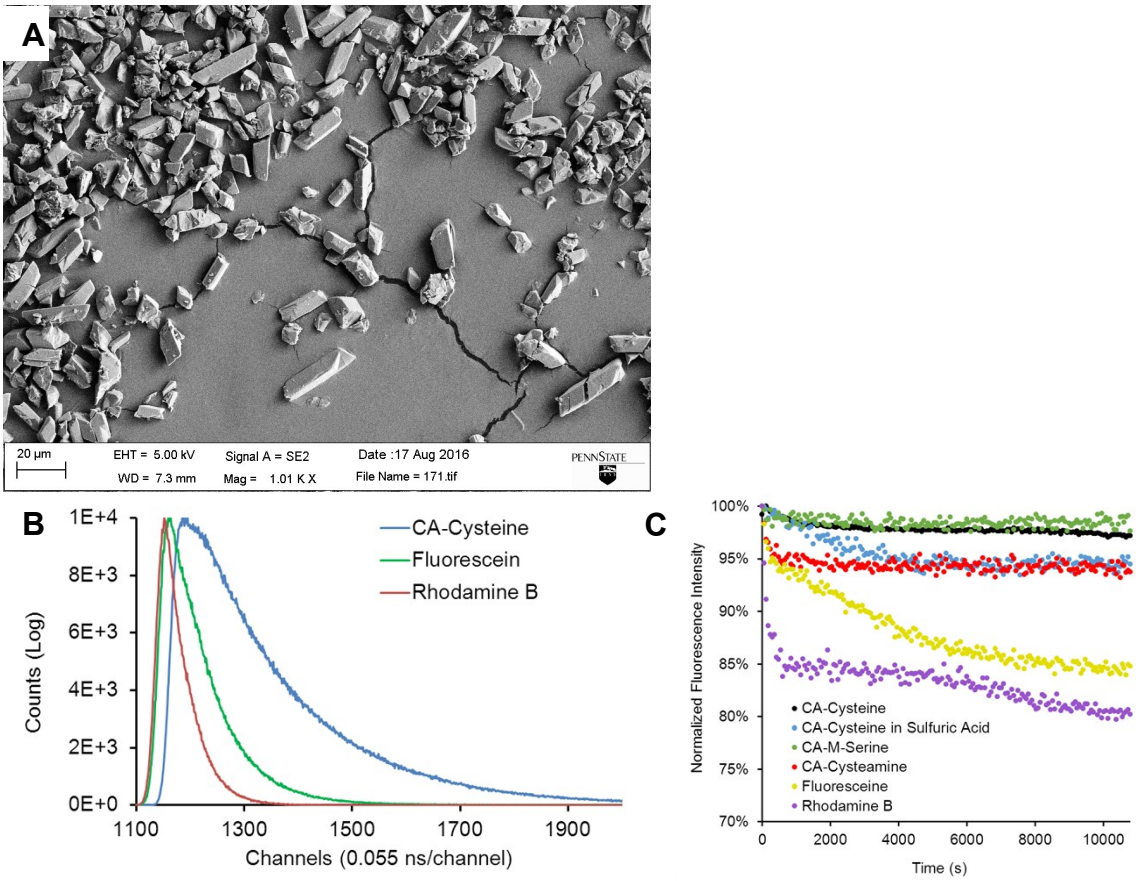

Figure S3. (A) Scanning electron microscope (SEM) image of CA-Cysteine. (B) Fluorescence lifetime decay curves of CA-Cysteine compared to those of traditional dyes Fluorescein and Rhodamine B **(C) Photostability of CFDs.** Normalized maximum fluorescence intensity of citrate-based fluorescence sensors compared to control dyes Rhodamine B and Fluorescein over 3 hours of continuous illumination at 1 nm excitation and 1 nm emission bandpass.

Table 1. Comparison of fluorescence properties of citrate-based fluorescence sensors compared to those of traditional dyes, Rhodamine B and Fluorescein**.**

Compound	Photobleaching (% degradation)	Quantum Yield	Lifetime
CA-Cysteine	2.9%	81.20%	10.06 ns
CA-Cysteamine	6.8%	78.02%	
CA-Methyl-Serine	2.4%	89.88%	
Rhodamine B	20.3%	70% [37]	1.75 ns
Fluorescein	16.1%	91% [37]	4.19 ns

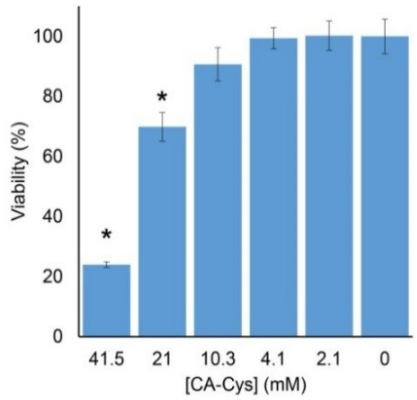

Figure S4. Cytotoxicity of CA-Cysteine on 3T3 mouse fibroblasts (CCK-8/assay, 24hr incubation) showing no statistically significant decrease ($p>0.05$) in cell viability up to a dosage of 10.3 mM compared to control, while dosages of 21 mM and 41.5 mM showed significance differences (* $p<0.05$).

Table 2. Commercial costs of existing fluorescence-based chloride sensors

Compound	Cost (ThermoFisher, as of 2016)
MQAE (N-(ethoxycarbonylmethyl)-6-methoxyquinolinium	\$197/100 mg [38]
SPQ (-methoxy-N-(3-sulfopropyl)quinolinium)	\$163/100 mg [39]
MEQ -methoxy-N-ethylquinolinium	\$129/100 mg [40]

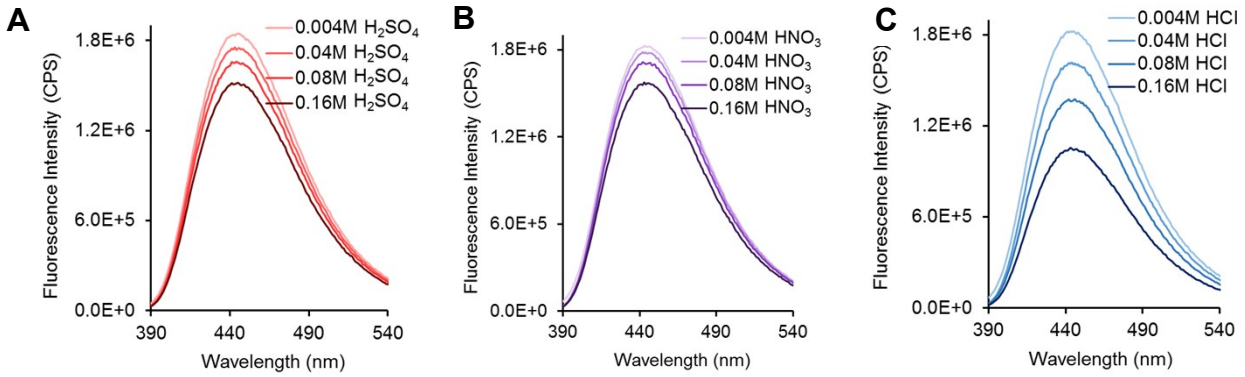

Figure S5. Chloride sensing "switches on" under acidic conditions. Emission spectra of CA-Cysteine measuring quenching rates of various strong acids H_2SO_4 (A), HNO_3 (B) and HCl (C) suggest that HCl dissociates into two quenchers.

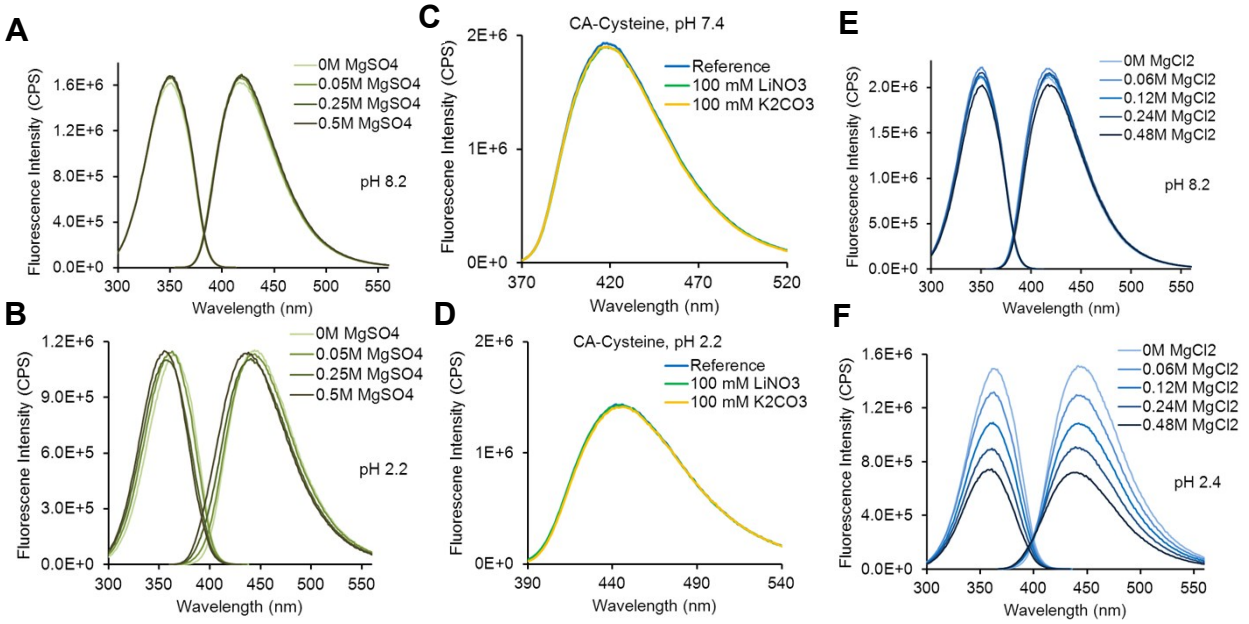

Figure S6. Chloride ions quench fluorescence only under high acidity. (A-F) Fluorescence Spectra of CA-Cysteine in $MgSO_4$ (A-B), $LiNO_3$ and K_2CO_3 (C-D) show absence of quenching under both low pH and high pH conditions, and likewise, $MgCl_2$ (E), by itself, does not quench fluorescence unless in acidic conditions (F).

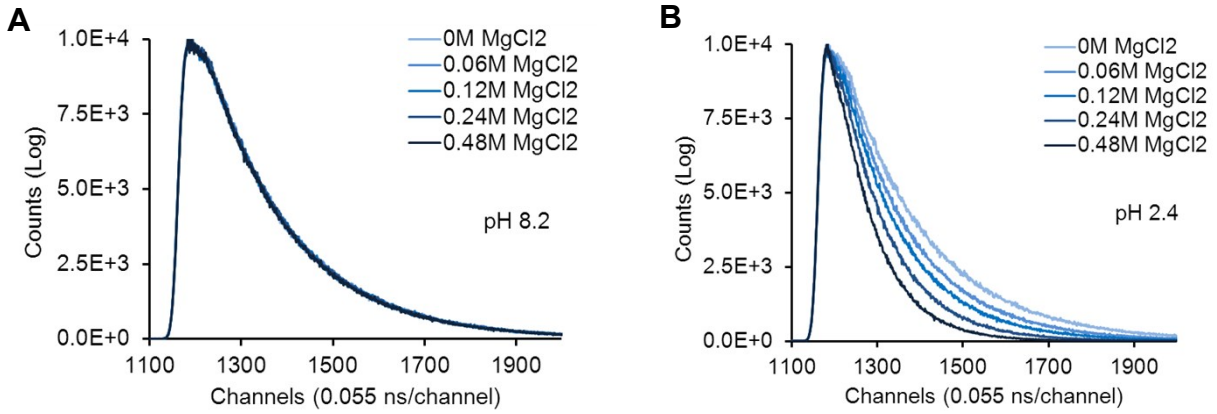

Figure S7. Lifetime decay plots show that quenching by $MgCl_2$ under acidic conditions is a dynamic quenching mechanism.

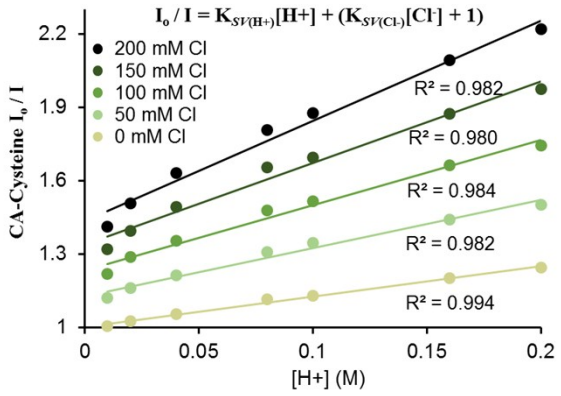

Figure S8. Stern-Volmer Plot of Quenched Lifetime versus [H^+] at Varying [Cl^-]. Data from Figure 1C was transposed to demonstrate the effects of [Cl-] on the proton-induced lifetime quenching. Non-linearity of SV plot suggests independence of $K_{SV(H+)}$ from [Cl^-].

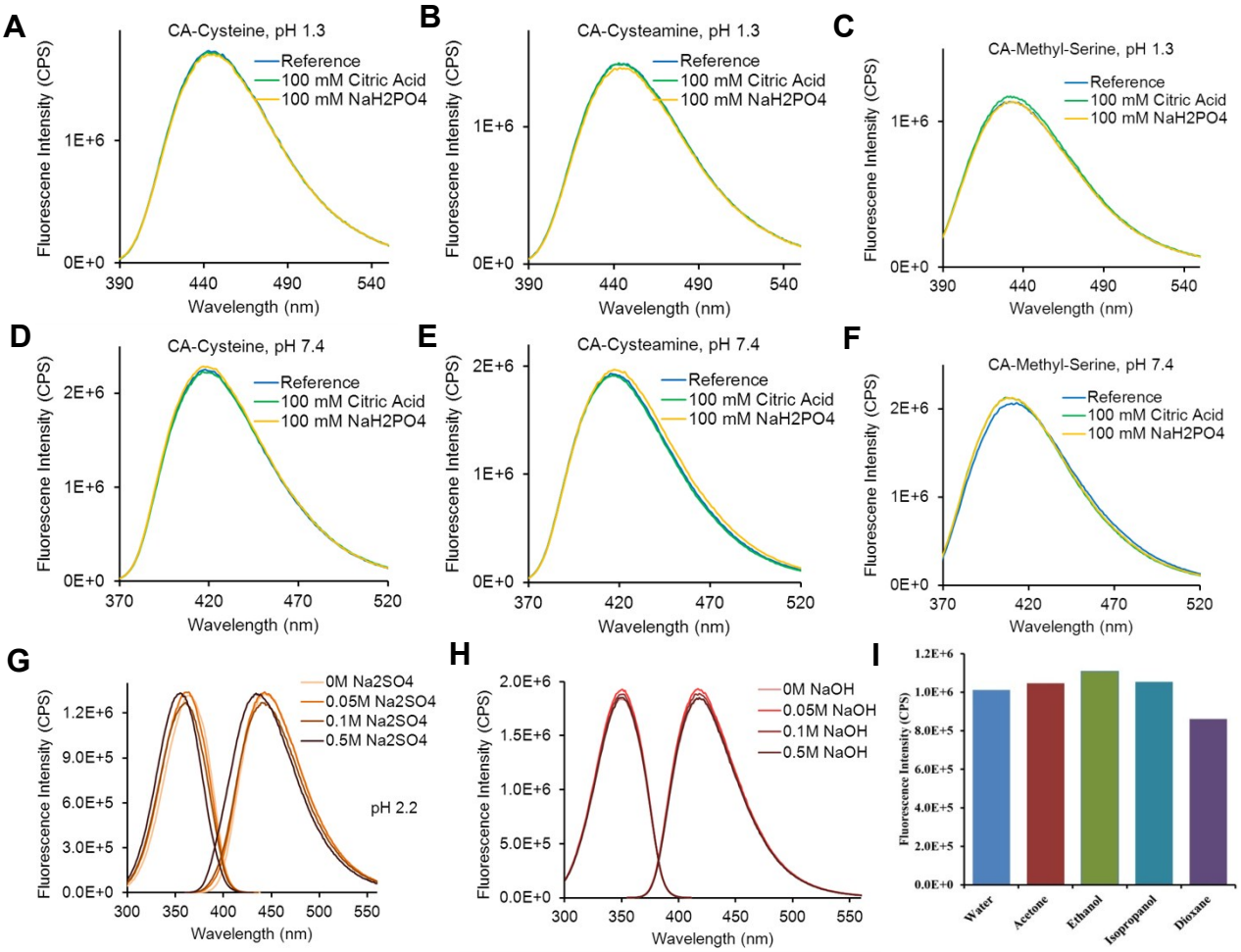

Figure S9. (A-H) Citrates, phosphates, lithium, potassium, nitrate, carbonate, sodium, and hydroxide ions do not quenching fluorescence for various citrate-based fluorescence sensors and under acidic and physiological conditions, validating the use of appropriate buffers and counter-ions. (I) Fluorescence intensity of CA-Cysteine in different solvents, demonstrating minimal quenching in dioxane, acetone, ethanol, isopropanol, and DMSO compared to that in water

	Chloridometer (QM)		CA-Cysteine	
	Average	Deviation	Average	Deviation
QM-1	23 mM	±5 mM	25.1 mM	±7.28 mM
QM-2	51 mM	±10.5 mM	47.5 mM	±8.75 mM
QM-3	106 mM	±21 mM	96.5 mM	±13.44 mM

Table S3. Comparison of measured chloride levels in sweat controls using CA-Cysteine versus a Chloridometer (QuantiMetrix)

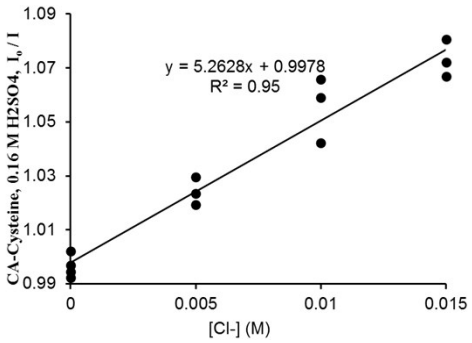

Figure S10. Standard curve was prepared with sodium chloride under 0.16M H_2SO_4, and the slope of 5.263 was used to determine chloride levels of sweat controls based on quenched intensity, then compared to mean and standard deviations reported by QuantiMetrix based on Chloridometer readings.

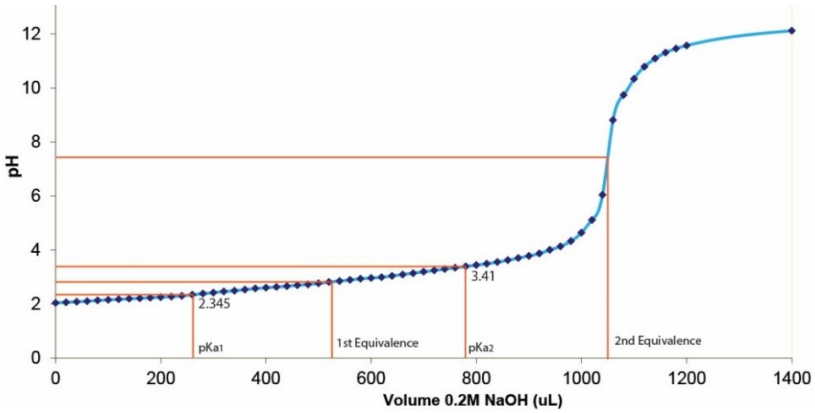

Figure S11. Titration of CA-Cysteine with NaOH revealed a diprotic acid. CA-Cysteine (25.79 mg) was titrated with NaOH (0.2M), resulting in an end inflection point of 1049. uL of NaOH determined from a first derivative plot of the titration curve. The long buffered region of the titration curve supports the presence of two carboxyl groups with close pKas that are overlapping the first inflection point. A molar mass value of 245.6 g/mol is obtained for CA-Cysteine when assuming a diprotic acid, close to the value of 241 g/mol as determined by LC-ESI-MS[21]. A pKa_1 value of 2.345 was assigned to the 3-carboxyl group, while a pKa_2 value of 3.41 was assigned to the 7-carboxyl group based on the reasoning that the 3-carboxyl is derived from and structurally similar to the α-carboxyl group of cysteine, while the 7-carboxyl is in a resonance-stabilized environment similar to that of benzoic acid.

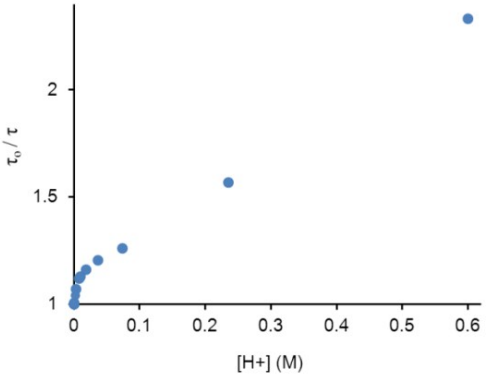

Figure S12: **Stern-Volmer lifetime plot** of CA-Cysteine quenching rates under increasing acidity, where quenching is quantified by the term τ_o/τ, which is equivalent to I_o/I or Φ_o/Φ depending on the instrument of detection. τ_o is defined as the fluorescence lifetime in the absence of quenchers, while τ is the fluorescence lifetime in the presence of quenchers. The plot reveals a linear, negative deviation of lifetime values from pH 2.3 (0.004M H_2SO_4) and below, accompanied by very low χ^2 values for 1-exponential decay, a textbook example of dynamic (excited state) quenching. Assuming CA-Cysteine is predominantly in its neutral state near pH 2.3, we postulate that the nonlinearity of the SV-plot above this pH is due to protolytic equilibria to other (anion and dianion) states, whereas linearity below pH 2.3 is due to excited state protonation of the 5-carbonyl (only occurring under high acidity after both carboxyls have been protonated).

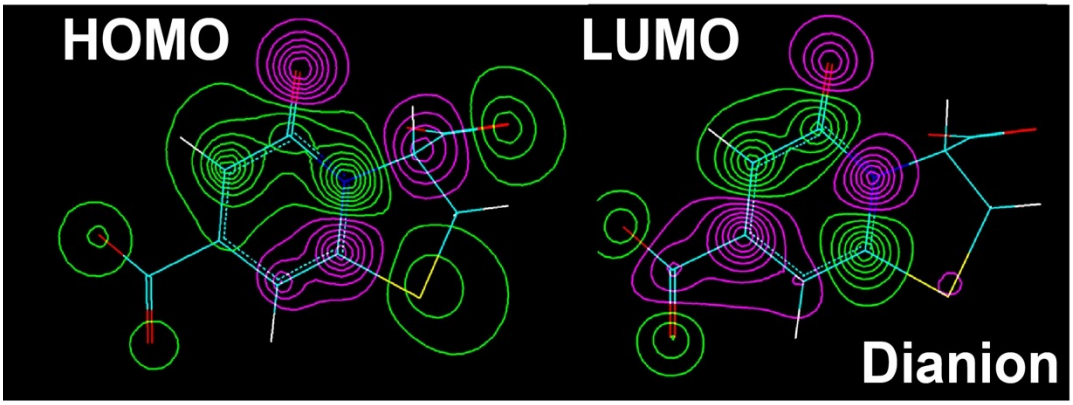

Figure S13. Energy level diagram of different protolytic states of CA-Cysteine. Compared to neutral state CA-Cysteine (Fig. 3B-C), a lower HOMO-LUMO gap (by 0.57 eV) in the dianion state is attributed to better stabilized LUMO energy levels.

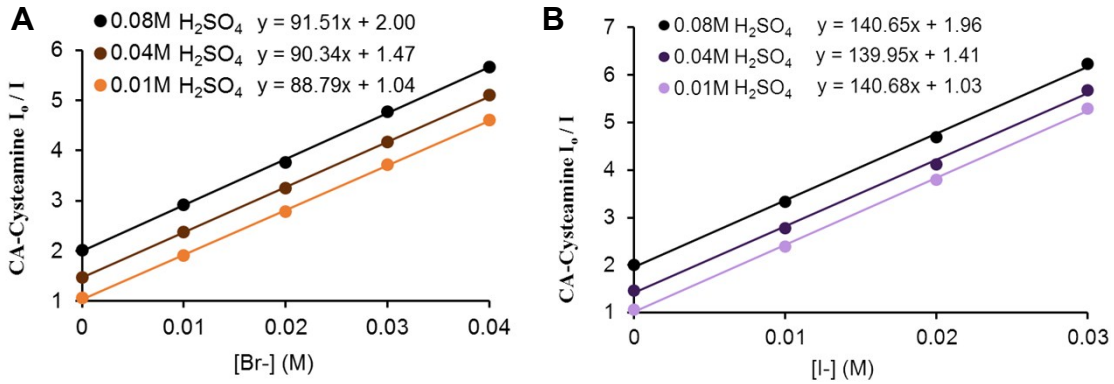

Figure S14. Bromide (A) and Iodide (B) sensitivity of CA-Cysteamine in sulfuric acid, $R^2 >$ 0.999 and $R^2 > 0.998$ respectively.

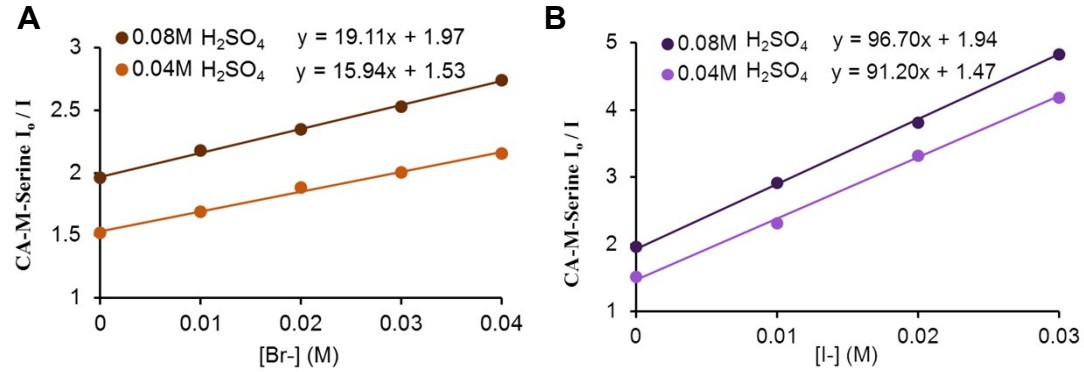

Figure S15. Bromide (A) and Iodide (B) sensitivity of CA-Methyl-Serine in sulfuric acid, $R^2 >$ 0.994 and $R^2 > 0.999$ respectively.

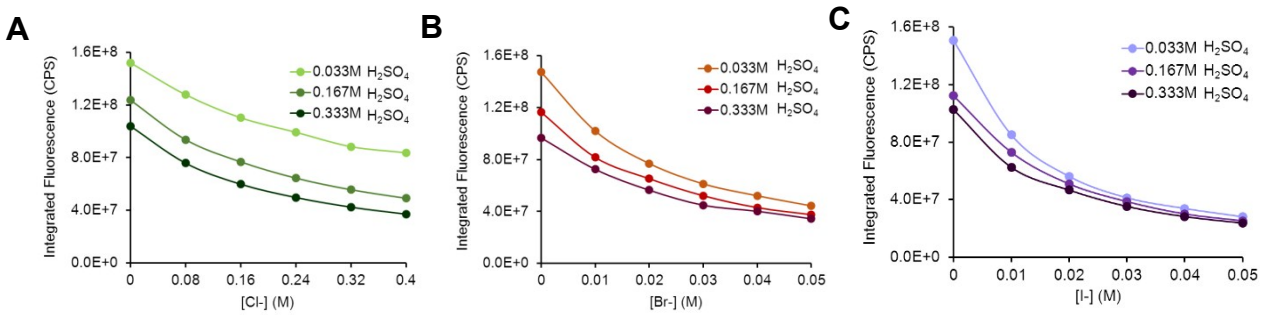

Figure S16. Integrated fluorescence intensities of CA-Cysteine demonstrate that halide sensitivities in different acidic conditions demonstrate different patterns of pH-dependence. CA-Cysteine quenched by chloride, bromide, and iodide demonstrate a diverging pattern for chloride sensitivity upon increasing acidity (a), and converging pattern for bromide (b) and iodide (c). Translated into Stern-Volmer plots, chloride Ksv would increasing significantly as acidity increases (Fig 4e), while bromide Ksv levels out to a constant Ksv at 0.04M H2SO4 (Fig 5A), and iodide Ksv levels out around 0.08M H2SO4 (Fig 5a).

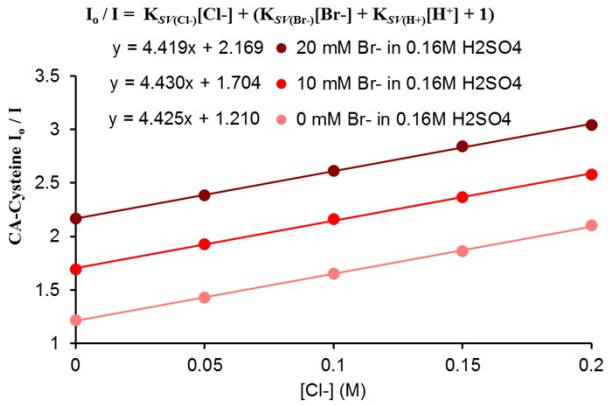

Figure S17. Halides are independent quenchers, demonstrated by quenching CA-Cysteine fluorescence with fixed LiBr concentrations while varying $MgCl_2$ levels, in contrast to the pH-dependence of chloride quenching, allowing for determination of multiple quencher concentrations based on a system using multiple fluorophores. $R^2 > 0.999$ for all fitted lines

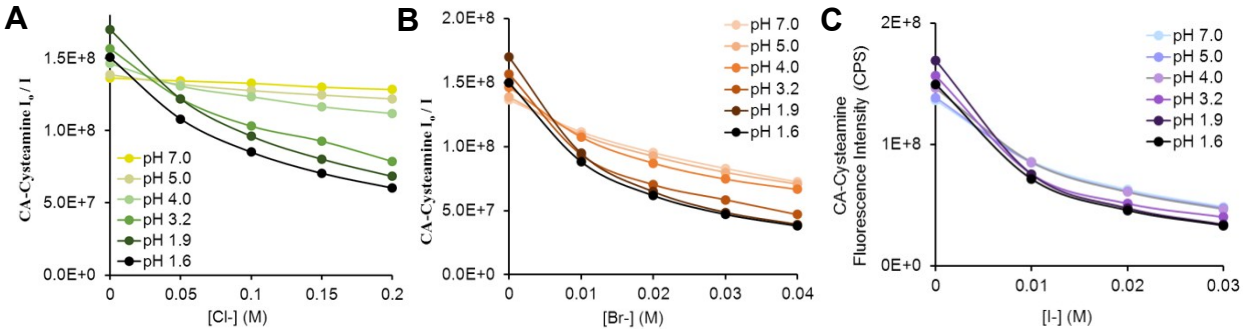

Figure S18. Integrated fluorescence intensities measuring chloride (A), bromide (B) and iodide (C) quenching rates of CA-Cysteamine at different pH, revealing a jump in halide sensitivity at the pKa of 7-carboxyl. For chloride, sensitivity continues to increase past this pKa, likely due to excited state protonation of 5-carbonyl.

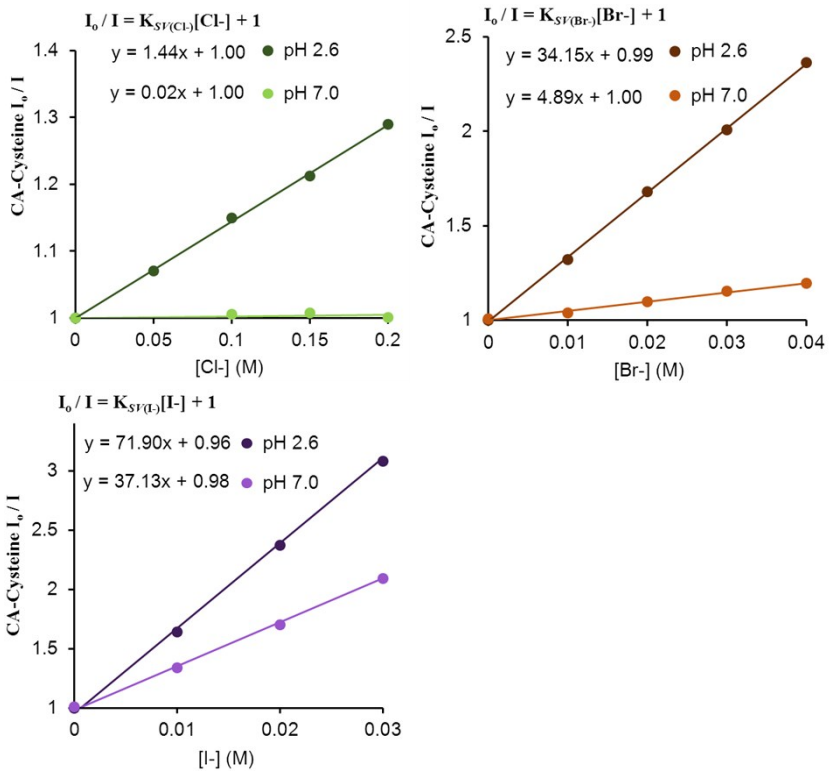

Figure S19. Halide Sensitivity of CA-Cysteine at Different pH. R^2=0.24 for Chloride at pH 7.0, R^2 = 0.999 for Chloride at pH 2.6, R^2>0.993 for Bromide, R^2>0.999 for Iodide. pH 6 and pH 7 made from 50mM phosphate buffer (Na2HPO4 and NaH2PO4), pH 2.6, 3.2, 4.0, 5.0 made from 50 mM Citric acid-NaH2PO4 buffer

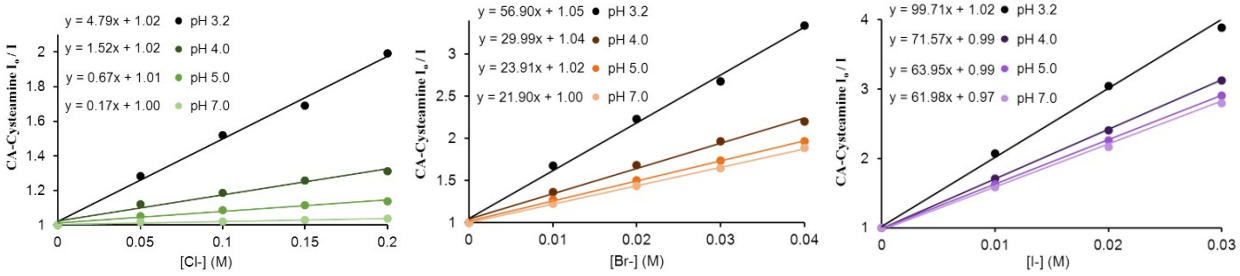

Figure S20. Halide Sensitivity of CA-Cysteamine at Different pH. R^2=0.957 for Chloride at pH 7.0, R^2 > 0.974 for Chloride at other pH, R^2>0.993 for Bromide, R^2>0.997 for Iodide

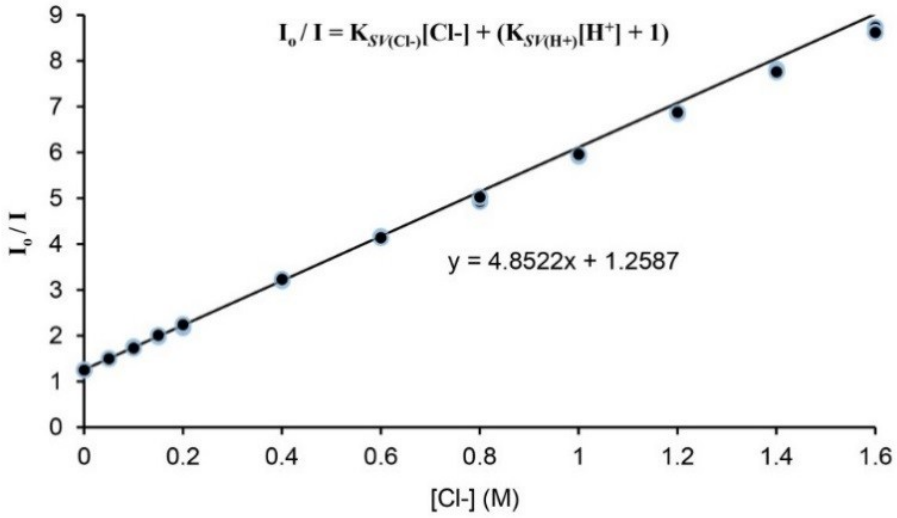

Figure S21. Upper limit of chloride detection for CA-Cysteine, where the Ksv determined from 0-200 mM chloride was extended to chloride concentrations of up to 1600 mM with three replicate samples for each concentration. The linearity of the Stern-Volmer plot was maintained up to 1400 mM with less than 4% error, i.e. expected chloride concentrations using a trend line determined from 0-200 mM chloride had less than 4% error compared to actual measured values.

Table S4: Useful Detection Limits of CAPS at various CFDs for Chloride, Bromide, and Iodide at different pH conditions, based on Signal to Noise ratio of 3 on Fluoromax-4.

Sensor Compound	Halide	pH Conditions	
CA-Cysteine	Chloride	pH 0.68 [a]	0.83 mM
		pH 7.0	120 mM
	Bromide	pH 1.33 [a]	59.1 uM
		pH 7.0	0.56 mM
	Iodide	pH 1.33 [a]	33.0 uM
		pH 7.0	74.4 uM
CA-Cysteamine	Chloride	pH 1.59 [a]	373 uM
		pH 5.0	4.1 mM
		pH 7.0	16.1 mM
	Bromide	pH 1.85 [a]	32.3 uM
		pH 5.0	116 uM
		pH 7.0	126 uM
	Iodide	pH 1.85 [a]	20.2 uM
		pH 5.0	43.2 uM
		pH 7.0	44.5uM

[a] optimal pH conditions determined from the Ksv and signal-to-noise ratio, according to equation S11 and S16

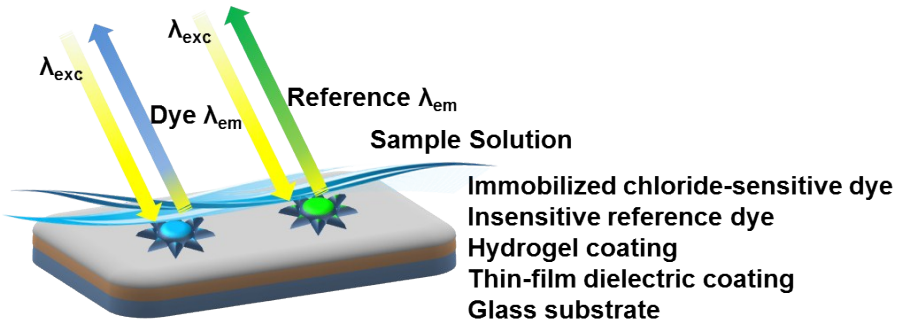

Figure S22. Schematics for real-time continuous monitoring, where citric acid-based sensors are immobilized onto a hydrogel for solid-state fluorescence along with a chloride-insensitive reference dye. Since dynamic quenching is a photophyical process that does not degrade the dye, real-time continuous monitoring is enabled using this method.

Section B: Derivation of Stern-Volmer equations

When a fluorophore of [F] absorbs light energy, excitation raises a sub-population of [F] to the excited state, [F*], which then rapidly lose energy along radiative relaxation (k_r) or non-radiative relaxation (k_{nr}) (Equation S1)[41]. If a quencher forms a complex with the excited fluorophore, an extra non-radiative component, k_q, is added to account for the additional relaxation pathway that is a function of quencher concentration and its association constant.

$$\frac{d[F*]}{dt} = -kr[F*] - knr[F*] - kq[Q][F*] \qquad (S1)$$

In lifetime measurements, equation S1 is given in the exponential form[41]:

$$[F*] = [F*]0\, e^{-(kr + knr + kq[Q])t} \qquad (S2)$$

From which the quenched and unquenched lifetimes, τ and τ_0, can be determined:

$$\tau = \frac{1}{kr + knr + kq[Q]} \quad , \quad \tau 0 = \frac{1}{kr + knr} \qquad (S3)$$

Thus the quenching of fluorescence can be quantitatively analyzed by comparing the affected lifetimes. The Stern-Volmer (SV) relationship is used to determine k_q, the bimolecular quenching rate constant for the diffusion coefficients of the fluorophore and quencher, by deriving a plot of τ_0/τ versus [Q]:

$$\frac{\tau 0}{\tau} = \frac{kr + knr + kq[Q]}{kr + knr} = 1 + \frac{kq[Q]}{kr + knr} = 1 + kq\tau 0[Q] = 1 + KSV[Q] \qquad (S4)$$

Thus the linear slope of the SV plot, K_{SV}, measures the efficiency of the quencher. Since sulfuric acid was used to study proton-induced quenching, the pH value was a better indicator of $[H^+]$ due to incomplete dissociation of sulfuric acid at high concentrations. In the case of multiple quenchers, as will be discussed in this paper, equation S1 must include additional k_q terms that result in modified form of equation S5 below:

$$\frac{\tau 0}{\tau} = \frac{kr + knr + kq1[Q1] + kq2[Q2]}{kr + knr} = 1 + kq1\tau 0[Q1] + kq2\tau 0[Q2] \qquad (S5)$$

If the two quenchers are act independently, the quencher of known quenching rate and concentration can be combined into the Y-intercept term in order to determine the quenching rate of the second, unknown quencher. The above equations are valid for all dynamic quenching processes, where the fluorophore is unaffected in the ground state, but forms excited state complexes that lead to additional non-radiative pathways, thereby affecting reducing the lifetime, quantum yield, and intensity of the emitting species. For such dynamic processes, the term τ_0/τ can be interchanged with quantum yield or intensity ratios (F_o/F), giving:

$$\frac{Io}{I} = \frac{\Phi 0}{\Phi} = 1 + KSV\,1[Q1] + KSV\,2[Q2] \qquad (S6)$$

We applied this concept in our clinical evaluations, such that samples diluted in dye and acid would exhibit fluorescence quenched by both protons and chloride. We defined the unquenched reference signal, I_o, as the fluorescence of neutral state CA-Cysteine at a pH value just following completion of the protolytic transition but before additional dynamic quenching effects materialize. According to the fluorescence lifetime study (Supplementary Figure S12), linearity of proton-induced dynamic quenching begins just after pH 2.2, where CA-Cysteine is expected to be predominantly in its neutral state.

Section C: Molecular mechanism

The intensity of absorption and emission is dependent on the transition dipole moment, which is in turn dependent on the polarizability of the conjugated system. Here, heteroatoms such as nitrogen and carbonyl are invaluable within the aromatic system as their high electronegativities allow greater change in charge redistribution. Most fluorophores with bright emission are able to achieve an internal charge transfer (ICT) state upon excitation, where a highly electronegative EDG donates electrons to a EWG, resulting in a strong optical transition with sharp peaks[20]. For CA-Cysteine, this charge separation seems to come from the transfer of electrons from the nitrogen to the ring as well as to the EWG carbonyl group, as Hyperchem modeling showed that the atomic charge density at the nitrogen changes from ~ -0.98 to -0.14 upon excitation. The pattern of electron acceptance among the EWGs depended on the protolytic state of CA-Cys, as mentioned earlier, but the carbonyl consistently changed from ~ -0.66 to -0.4 upon excitation. Therefore the ground state of CA-Cysteine seems to favor the keto resonance structure with the wavefunction polarized onto the nitrogen, while the excited state of CA-Cysteine seems to favor the enol structure through ICT.

Such placement of electronegative heteroatoms and EWG groups are particularly important in the formation of an excited ICT state favoring the charge separated enol resonance structure. This structure has significant influence on the excited state pKa of the 5-carbonyl oxygen, as the aromatic ring stabilizes the enolate and makes the protonated enol less acidic. The increase in excited state pKa is even further enhanced by the increase in buffer capacity under high [H_2SO_4], where partial dissociation of the diprotic acid at very low pH would increase the rate of excited state buffer-catalyzed protonation. Both factors may raise the expected pKa of -0.5 for the carbonyl oxygen of an amide group.

Next, we speculate that protonation of the 5-carbonyl induces out-of-plane vibrational relaxation resembling a milder form of TICT. In a study of pyridone derivatives with various ring substituents, Guzzo et al. reported that substituents that increase the planarity and rigidity of the aromatic ring, such as through internal hydrogen bonding, minimized the rate of internal conversion by reducing out-of-plane modes of molecular vibration, which would then reduce interactions between states[42]. This would be particularly true for heteroaromatics, due to the proximity of n-π^* and π-π^* states. Likewise,

As the carbonyl is originally sp2 hybridized, with its lone pair electrons planar with the aromatic ring due to contributions from the keto resonance form, it is hypothesized that protonation of this carbonyl leads to a greater sp3 character on the oxygen, resulting in significant loss of planarity and rigidity of the overall structure. Molecular modeling of the protonated enol structure of CA-Cysteine supports this hypothesis, as the carbonyl bond length has increased single-bond character upon protonation (1.22 Å in the enolate, versus 1.327 Å in the protonated enol). This loss of planarity within the 2-pyridone ring may enhance rates of interconversion or intersystem crossing, leading to proton-induced quenching of fluorescence and lifetimes as was observed.

Section D: Selective detection methods

For a simple demonstration of multi-halide sensing based on CA-Cysteine, we simulated sea water diluted 1:3, containing final concentrations of 187.3 mM chloride and 0.2895 mM bromide. Sea water has a Cl:Br ratio of 647:1, so trace bromide would normally contribute to positive error in chloride readings, while bulk interfering chloride would make sensitive bromide measurements difficult. To demonstrate selective chloride and bromide determination, we modified sensing protocols for the detection of two halides at two pH conditions, shown below:

$$\frac{I\mathrm{O}}{I0.01\mathrm{M\ H2SO4}} = K'\mathrm{SV(Cl-)[Cl-]} + K'\mathrm{SV(Br-)[Br-]} + K'\mathrm{SV(H+)}[H+] + 1$$
$$\frac{I\mathrm{O}}{I0.16\mathrm{M\ H2SO4}} = K''\mathrm{SV(Cl-)[Cl-]} + K''\mathrm{SV(Br-)[Br-]} + K''\mathrm{SV(H+)}[H+] + 1 \quad \text{(S7)}$$

The first step was to create standard curves of chloride and bromide at two pH conditions. To shorten this standardization process, we referred to our earlier systematic study cataloguing halide sensitivities of CA-Cysteine at different pH (Figure 4e and 5a), noting K_{SV} values of 2.0242 for chloride at 0.01M H_2SO_4 and 4.4309 at 0.16M H_2SO_4, as well as K_{SV} values of 44.008 for bromide at 0.01M H_2SO_4 and 49.984 at 0.16M H_2SO_4, and then re-measured only the unquenched reference signal and the reference signal quenched by sulfuric acid prior to measuring the unknown sample (sea water), to account for variations in machine sensitivity or dye concentrations. Doing so also provided the ($K_{SV(H+)}[H^+] + 1$) term of 1.026 at 0.01M H_2SO_4 and 1.219 at 0.16M H_2SO_4. Next, we measured our unknown sample (simulated sea water diluted 1:3) under 0.01M H_2SO_4 and 0.16M H_2SO_4, obtaining a Io/I value of 1.416 at 0.01M H_2SO_4 and 2.061 at 0.16M H_2SO_4. Plugging these values into the equation above, we solved for chloride and bromide concentrations, obtaining 187.1 mM for chloride and 0.268 mM for bromide after factoring in dilution, corresponding to percent errors of 0.1% and 7.4% respectively. As mentioned, this method is important not only for detecting trace halides in the presence of bulk interfering halides, but also in reducing positive error in bulk halide measurement from the trace halides themselves. In this case, if bromide interference is not taken into account, sea water at a Cl:Br ratio of 647:1 would result chloride measurements of 193.9 mM at 0.01M H2SO4 and [Cl-] = 191.1 mM at 0.16M H2SO4, corresponding to positive errors of 3.55% and 2.05% respectively, highlighting the importance of selective detection methods.

To visually describe the inner workings of this multi-halide detection method, we created a standard curve for sea water at 0.01M H_2SO_4 and 0.16M H_2SO_4 in Figure S26 by measuring quenched intensities of sea water diluted 1/12, 2/12, 3/12, and 4/12 and setting the x-axis as the expected chloride levels in each measurement. Since halides are independent quenchers, K_{SV} values are additive, so for the Cl:Br ratio of 647:1 in sea water,

$$K_{SV(\text{sea-water})}[\text{Sea-water}] = K_{SV(Cl-)}[Cl^-] + (K_{SV(Br-)}/647)\,[Br^-] \quad \text{(S8)}$$

Thus at 0.01M H_2SO_4, the measured slope of 2.0964 for sea water originates from the contribution of chloride K_{SV} of 2.0242 and of bromide K_{SV} of 44.08/647, which adds up close to an expected combined K_{SV} of 2.092. In other words, measuring an unknown sample essentially outputs this combined slope from which we can separate the extent of contribution from each halide by solving two equations, which works because chloride and bromide sensitivities change disproportionately at different pH.

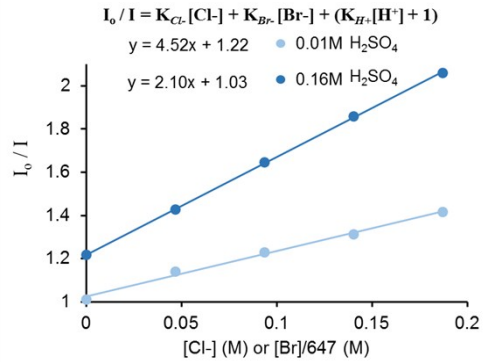

Figure S21: Determination of concentrations of two halides, $R^2 > 0.994$

Section E: Combining interfering quencher terms

For selective chloride or bromide detection, combining the quenching contribution of other halides will greatly simplify the detection method. Wolfbeis proposed that the identity or sensitivity of *n* interferents can be taken into account by *n* measurements[43]. Here, we propose that all other halides can be combined into a single term so that a specific halide in a complex sample can be measured with only two measurements producing two equations to solve for two unknowns: the concentration of the desired halide and the combined interferent term. The mathematical proof is outlined below:

- For multiple quenchers, where A and B are unknown interferents
  - $\frac{IO}{I} = K\text{SV(Cl -)}[\text{Cl - }] + K\text{SV(A)}[A] + K\text{SV(B)}[B] + K\text{SV(H +)}[\text{H + }] + 1$
- At constant pH, $(K\text{SV(H +)}[H +] + 1) = C$ (a constant)
  - $\frac{IO}{I} = K\text{SV(Cl -)}[\text{Cl - }] + K\text{SV(A)}[A] + K\text{SV(B)}[B] + C$
- In a standardized sample with [Cl-] = 0.1 M, [A] = [a], [B] = [b]
  - $\frac{IO}{I} = K\text{SV(Cl -)}[0.1] + K\text{SV(A)}[a] + K\text{SV(B)}[b] + C$
- Let [0.1] = α[a], and [0.1] = β[b], (α/β are proportionality constants)
  - $\frac{IO}{I} = K\text{SV(Cl -)}[0.1] + \frac{K\text{SV(A)}}{\alpha}[0.1] + \frac{K\text{SV(B)}}{\beta}[0.1] + C$
  - $\frac{IO}{I} = K\text{SV(Cl -)}[0.1] + \frac{\beta K\text{SV(A)} + \alpha K\text{SV(B)}}{\alpha\beta}[0.1] + C$
  - $\frac{IO}{I} = K\text{SV(Cl -)}[0.1] + K\text{SV(int)}[0.1] + C$
- Solve for $K'\text{SV(int)}$ and $K''\text{SV(int)}$ at two different pH
- In unknown sample, let [Cl-] = W*[0.1], [A] = X*[a], [B] = Y*[b]
  - $\frac{IO}{I} = K\text{SV(Cl -)}[0.1]W + K\text{SV(A)}[a]X + K\text{SV(B)}[b]Y + C$
- Let [0.1] = α[a], and [0.1] = β[b],
  - $\frac{IO}{I} = K\text{SV(Cl -)}[0.1]W + \frac{K\text{SV(A)}}{\alpha}[0.1]X + \frac{K\text{SV(B)}}{\beta}[0.1]Y + C$
  - $\frac{IO}{I} = K\text{SV(Cl -)}[0.1]W + \frac{\beta K\text{SV(A)} + \alpha K\text{SV(B)}}{\alpha\beta}[0.1]XY + C$
  - $\frac{IO}{I} = K\text{SV(Cl -)}[0.1]W + K\text{SV(int)}[0.1]Z + C$

- Solve for W and Z (system of two equations measured at two pH)

Generally, this proof demonstrates that any number of quenchers can in fact be combined into a single term without identifying, or measuring the sensitivities of, or measuring concentrations of each individual quencher.

Section F: Detection Limits

As the Stern-Volmer equation is a linear representation of the dynamic quenching phenomena, lower limits are essentially bounded by the detection limit of the fluorescence instrument, while upper limits stem from nonlinearity in the Stern-Volmer relation which may result from ionic strength effects at particularly high halide concentrations[44]. The lower limit of detection is defined according to desired signal to noise ratio (S/N), defined as the mean of signal strength over its Root Mean Square (RMS) error[45]. When observing fluorescence quenching, the lower limit of detection is bounded by the smallest discernible difference in unquenched versus quenched maximum or integrated fluorescence signals. Hence, the signal is defined as the ratio of the unquenched and quenched fluorescence, while noise is the variability of the integrated fluorescence from sample to sample, i.e. the RMS error[46]:

$$Noise = RMS = \sqrt{\frac{\sum_{i=1} (X\mathrm{i} - \bar{X})}{n}} \qquad (S9)$$

In addition, signal is defined as $S = I\mathrm{o} - I$

The Stern-Volmer equation, $I_o / I = 1 + K_{SV}[Q]$, can be plugged in to derive equation S9[15,47]:

$$S = I\mathrm{o}\left(1 - \frac{1}{(1 + K\mathrm{SV}[Q])}\right) \qquad (S10)$$

When determining the limit of detection, where the signal is defined as the smallest discernible difference between the unquenched and quenched signals, one can assume that the noise of the unquenched signal is approximately equal to the noise of the quenched signal (i.e. as $I \rightarrow I_o$, and $S \rightarrow 0$, then $N \rightarrow N_o$)[46]. Thus, the signal to noise ratio is simplified to equation S10[47]:

$$\frac{S}{N} = \frac{I\mathrm{o}}{N\mathrm{o}}\left(1 - \frac{1}{(1 + K\mathrm{SV}[Q])}\right) \qquad (S11)$$

This method is valid for all measurements in physiological pH where proton quenching is not effective. However, in the halide sensing methods listed above where fluorescence is measured at a fixed highly acidic solution, proton quenching results in:

$$S = I\mathrm{pH} - I\mathrm{pH,\,Cl} \qquad (S12)$$

Where $I_{pH,Cl}$ and I_{pH} are both measured at the same pH, with and without chloride respectively, and are defined by the SV equation S12 and S13:

$$\frac{I\mathrm{o}}{I\mathrm{pH}} = K\mathrm{SV(H+)}[H+] + 1 \qquad (S13)$$

$$\frac{I\mathrm{o}}{I\mathrm{pH,\,Cl}} = K\mathrm{SV(H+)}[H+] + K\mathrm{SV(Cl-)}[Cl-] + 1 \qquad (S14)$$

Dividing equation S13 by S12,

$$\frac{I\mathrm{pH}}{I\mathrm{pH,\,Cl}} = 1 + \frac{K\mathrm{SV(Cl-)}[Cl-]}{K\mathrm{SV(H+)}[H+] + 1} \qquad (S15)$$

Thus in highly acidic solutions, equation S10 is modified to:

$$\frac{S}{N} = \frac{I\mathrm{pH}}{N\mathrm{o}}\left(1 - \frac{1}{(1 + \frac{K\mathrm{SV(Cl-)}[Cl-]}{K\mathrm{SV(H+)}[H+] + 1})}\right) \qquad (S16)$$

To determine N_o from the RMS error of integrated unquenched fluorescence, data was collected by making 36 mL of CA-Cysteine in distilled water at a final absorbance of 0.10, covered in foil. The first 5 mL of CA-Cysteine was used to rinse the cuvette and to measure the R1 of the fluorometer until the signals stabilized (kinetics, measured every minute for roughly 20 minutes). Three preliminary fluorescence measurements were run with the rinse solution to ensure signal consistency. Next, 10 x 3.000 mL samples of CA-Cysteine were measured at 1.2 nm excitation and emission slit widths (which were maintained throughout all experiments in this study), and emission was collected at 350 nm excitation. Each sample was discarded after measurement to eliminate photobleaching effects. Integrated fluorescence was calculated over 360 – 580 nm. These procedures were also repeated for CA-Cysteine in 0.16M sulfuric acid, except CA-Cysteine absorbance of 0.15 was used.

The I_o / N_o value of CA-Cysteine using Fluoromax-4 was determined to be 1089.5 based on the integrated fluorescence based on 10 replicate samples as described. This value was plugged into equation S10 to predict the minimum concentration of halide that would yield an average signal to noise ratio of 3 to estimate the detection limit of the fluorescence quenching system. However, for highly acidic conditions (at 0.08M H2SO4 and above), fluorescence intensity is significantly quenched by protons, requiring a 50% higher concentration of CA-Cysteine to achieve the same I_o. The noise under 0.16M H2SO4 was not significantly different, with a I_{pH} / N_o value of 939.7 based on integrated fluorescence. This value was used to find detection limits for sulfuric acid concentrations of 0.08M and higher.

Additional References

(37) Brouwer, Albert M. "Standards for photoluminescence quantum yield measurements in solution (IUPAC Technical Report)." Pure and Applied Chemistry 83.12 (2011): 2213-2228.
(38) "MQAE (N-(Ethoxycarbonylmethyl)-6-Methoxyquinolinium Bromide)." Thermo Fisher Scientific. N.p., 2016. Web. 16 Aug. 2016.
(39) "SPQ (6-Methoxy-N-(3-Sulfopropyl)Quinolinium, Inner Salt)." Thermo Fisher Scientific. N.p., 2016. Web. 16 Aug. 2016.
(40) "MEQ (6-Methoxy-N-Ethylquinolinium Iodide)." Thermo Fisher Scientific. N.p., 2016. Web. 16 Aug. 2016.
(41) Grubbs T. Fluorescence Lifetimes and Dynamic Quenching: Stetson University; 2015.
(42) Guzzo AV, Nelson DA. RADIATIONLESS DEACTIVATION AND FLUORESCENCE OF SELECTED PYRIDONES. Photochemistry and Photobiology. 1992;55:665-70.
(43) Wolfbeis, Otto S., and Edmund Urbano. "Method for fluorometric determination of the concentrations of substances in a sample and arrangement for implementing this method." U.S. Patent No. 4,580,059. 1 Apr. 1986.
(44) Hoffman MZ, et al. Rate constants for the quenching of excited states of metal complexes in fluid solution. Journal of physical and chemical reference data 1989;18.1:219-543.
(45) Holler FJ, Douglas A. Skoog, and Stanley R. Crouch. Principles of Instrumental Analysis. 6th ed: Cengage Learning 2007.
(46) Signal to Noise Determination for PTI Quantamaster Fluorometer, PTI technical note. Photon Technology International, HORIBA; 2011.
(47) Goodpaster JV, and Victoria L. McGuffin. Fluorescence quenching as an indirect detection method for nitrated explosives. Analytical chemistry. 2001;73.9:2004-11.